*Applied Mathematics, Modeling and Computer Simulation*
*C. Chen (Ed.)*
*© 2022 The authors and IOS Press.*
*This article is published online with Open Access by IOS Press and distributed under the terms of the Creative Commons Attribution Non-Commercial License 4.0 (CC BY-NC 4.0).*
*doi:10.3233/ATDE220038*

# Simulation and Experiment of Dual-Frequency Isolator for Variable Speed Helicopter

Zhizhuang FENG[1], Chen LIU, Zhenkun LI, Longtao XING, Qiyou CHENG
*China Helicopter Research and Development Institute, Jingdezhen 333001, China*

**Abstract.** In order to reduce the two main vibration frequency of the variable speed helicopter, an anti-resonance vibration isolator with double frequency vibration isolation is designed. First, the dynamic formula of the dual frequency vibration isolator was deduced based on the traditional dynamic anti-resonance theory. With the formula, the natural frequency, antiresonant frequency and transmissivity of the isolator are obtained. Then, the sensitivity of the performance and efficiency for the isolator is analyzed. The effects of design parameters such as secondary spring stiffness and secondary vibration isolation mass on the natural frequency and vibration isolation frequency of the isolator are obtained. The property test and vibration test are carried out. The calculation and test results show that the isolator has two vibration isolation frequency. The secondary vibration isolation efficiency is more than 60%, and the antiresonance frequency and efficiency of the isolator are both affected by the design parameters.

**Keywords.** Variable speed, double frequency, dynamical model, sensibility, test

## 1. Introduction

The vibration problem has plagued the development of helicopters since their birth. The vibration caused by the load of the rotor system, mainly NΩ, is the main concern [1]. Different from traditional helicopters, the variable-speed coaxial high-speed helicopter includes two mode in the entire mission profile. During the high-speed forward flight mode, the rotor speed needs to be reduced to avoid the shock stall of the forward blades [2], which brings about the frequency change of the rotor vibration load[3], resulting in the change of the vibration frequency[4]. Take the American X2[5] technical demonstrator as an example, the rotor speed of the aircraft in the hovering state is 446rpm. When the aircraft flies forward at high speed, the rotor speed drops to 360rpm. Reducing the rotation speed of the rotor changes the vibration frequency. Compared with the traditional helicopter, the vibration of the variable speed helicopter contains two frequency values.

For the need of multi-frequency vibration control, the traditional single-frequency passive vibration absorber can no longer meet the requirements. Active vibration isolators [6, 7] and self-tuning vibration isolators [8, 9] are the main approaches. Active vibration isolators [10] increase the vibration control effectiveness however does no

[1] Corresponding Author, Zhizhuang FENG, Helicopter Research and Development Center, Airport, Tianjin, China; E-mail: 463780298@qq.com.

effect on increasing the bandwidth, which also results in massive energy and mass cost. The auto-tuning isolator [11] greatly broadens the damping frequency bandwidth but could not increase the effect of vibration reduction, and the additional mechanical structure will also reduce the reliability of the isolator.

The dual-frequency vibration isolator, installed between the vibration source and the object, is a type of passive vibration isolation device for the transmission channel. According to the requirements of the vibration isolation frequency, it could be designed as a dynamic anti-resonance device with two optimal vibration isolation frequencies. Similar to the mechanism of the dynamic anti-resonance device, it could be a potential vibration reduction technology for variable speed rotors.

## 2. Dynamical Modelling of the Dual-Frequency Isolator

### *2.1. Design of the Dual-Frequency Isolator*

Take a variable-speed coaxial high-speed helicopter as an example. The rotor speed state is $\Omega_1$ in the hovering, and drops to $\Omega_2$ in flying forward at high speed. The excitation frequencies acts on the rotor system are $\omega_1$ and $\omega_2$. Changes in the main vibration frequency before and after high-speed flight.

Based on the mechanism of the single-frequency dynamic anti-resonance[12], a dual-frequency vibration isolation device with two-stage vibration isolation is proposed. The schematic diagram of the undamped dynamic anti-resonance device is shown in figure 1. The spring vibrating system consists of mass $m_t$, spring $k_1$ and mass $m_2$ and a lever system with amplification effect to absorb vibration energy. And vibration isolation under different excitation frequencies could be realized.

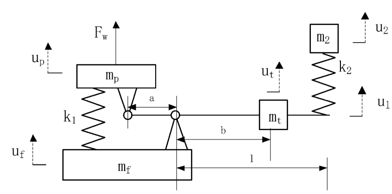


**Figure 1.** Schematic diagram of dual-frequency vibration isolator.

### *2.2. Dynamical Modelling*

Assuming that N dual-frequency vibration isolators are mounted on the transmission path between the helicopter rotor system and the fuselage, the total weight of the rotor system is $N \cdot m_p$, the total weight of the fuselage is $N \cdot m_f$, and the mechanical model of a single vibration isolator without damping could be simplified as figure 1.

$F_w$ is the external excitation force acting on a single vibration isolator, $m_t$ is the primary vibration isolation mass, $m_2$ is the secondary vibration isolation mass, $k_1$ is the primary spring stiffness, $k_2$ is the secondary spring stiffness; $u_p$, $u_f$, $u_1$, $u_2$ are the displacement of the rotor end, the fuselage end, the first-level vibration isolation mass and the second-level vibration isolation mass, respectively. And a, b, and l consists of the three-section lever system with different magnification ratios.

Applying the small-angle assumption for the movement of the lever system, one has,

$$\frac{u_f - u_p}{a} = \frac{u_t - u_f}{b} = \frac{u_l - u_f}{l} \tag{1}$$

Introducing the first-level amplification ratio $R_1$ and second-level amplification ratio $R_2$,

$$R_1 = \frac{b}{a} \quad , \quad R_2 = \frac{l}{b} \quad , \quad u_f = \frac{R_1 u_p + u_t}{R_1 + 1} \quad , \quad u_l = R_2 u_t + (1 - R_2) u_f \tag{2}$$

Ignoring the lever mass and rotational friction, the kinetic energy T and potential energy V of the system are written as,

$$T = \frac{1}{2} m_f \dot{u}_f^2 + \frac{1}{2} m_p \dot{u}_p^2 + \frac{1}{2} m_t \dot{u}_t^2 + \frac{1}{2} m_2 \dot{u}_2^2 \quad , \quad V = \frac{1}{2} k_1 (u_p - u_f)^2 + \frac{1}{2} k_2 (u_l - u_2)^2 \tag{3}$$

Substituting $u_f$ and $u_l$ into the above equations yields,

$$T = \frac{1}{2} m_f \left(\frac{R_1 \dot{u}_p + \dot{u}_t}{R_1 + 1}\right)^2 + \frac{1}{2} m_p \dot{u}_p^2 + \frac{1}{2} m_t \dot{u}_t^2 + \frac{1}{2} m_2 \dot{u}_2^2 \quad , \quad V = \frac{1}{2} k_1 \left(\frac{u_p - u_t}{R_1 + 1}\right)^2 + \frac{1}{2} k_2 \left[ R_2 u_t + (1 - R_2) \frac{R_1 u_p + u_t}{R_1 + 1} - u_2 \right]^2 \tag{4}$$

Applying the Lagrange equation and the governing equations of the system are obtained,

$$\frac{d}{dt}\left(\frac{\partial T}{\partial \dot{u}_p}\right) = [m_p + \frac{R_1^2 m_f}{(R_1+1)^2}] \ddot{u}_p + \frac{R_1 m_f}{(R_1+1)^2} \ddot{u}_t \ , \ \frac{d}{dt}\left(\frac{\partial T}{\partial \dot{u}_t}\right) = \frac{R_1 m_f}{(R_1+1)^2} \ddot{u}_p + \left[ m_t + \frac{m_f}{(R_1+1)^2} \right] \ddot{u}_t \ , \ \frac{d}{dt}\left(\frac{\partial T}{\partial \dot{u}_2}\right) = m_2 \ddot{u}_2 \tag{5}$$

$$\frac{\partial V}{\partial u_p} = \frac{k_1 + k_2 R_1^2 (R_2 - 1)^2}{(R_1+1)^2} u_p - \frac{k_1 + k_2 R_1 (R_2 - R_1 R_2 - 1 + R_1 R_2^2)}{(R_1+1)^2} u_t + \frac{k_2 R_1 (R_2 - 1)}{R_1 + 1} u_2 \tag{6}$$

$$\frac{\partial V}{\partial u_t} = -\frac{k_1 + k_2 R_1 (R_2 - R_1 R_2 - 1 + R_1 R_2^2)}{(R_1+1)^2} u_p + \frac{k_1 + k_2 (R_2 R_1 + 1)^2}{(R_1+1)^2} u_t - \frac{k_2 (R_2 R_1 + 1)}{R_1 + 1} u_2 \tag{7}$$

$$\frac{\partial V}{\partial u_2} = \frac{k_2 R_1 (R_2 - 1)}{R_1 + 1} u_p - \frac{k_2 (R_2 R_1 + 1)}{R_1 + 1} u_t + k_2 u_2 \tag{8}$$

Rewritten the above equations in matrix form,

$$\begin{bmatrix} \frac{k_1 + k_2 R_1^2 (R_2-1)^2}{(R_1+1)^2} & -\frac{k_1 + k_2 R_1 (R_2 - R_1 R_2 - 1 + R_1 R_2^2)}{(R_1+1)^2} & \frac{k_2 R_1 (R_2 - 1)}{R_1+1} \\ -\frac{k_1 + k_2 R_1 (R_2 - R_1 R_2 - 1 + R_1 R_2^2)}{(R_1+1)^2} & \frac{k_1 + k_2 (R_2 R_1 + 1)^2}{(R_1+1)^2} & -\frac{k_2 (R_2 R_1 + 1)}{R_1+1} \\ \frac{k_2 R_1 (R_2 - 1)}{R_1+1} & -\frac{k_2 (R_2 R_1 + 1)}{R_1+1} & k_2 \end{bmatrix} \begin{bmatrix} u_p \\ u_t \\ u_2 \end{bmatrix} + \begin{bmatrix} m_p + \frac{R_1^2 m_f}{(R_1+1)^2} & \frac{R_1 m_f}{(R_1+1)^2} & 0 \\ \frac{R_1 m_f}{(R_1+1)^2} & m_t + \frac{m_f}{(R_1+1)^2} & \\ & & m_2 \end{bmatrix} \begin{bmatrix} \ddot{u}_p \\ \ddot{u}_t \\ \ddot{u}_2 \end{bmatrix} = \begin{bmatrix} F_w \\ 0 \\ 0 \end{bmatrix} \tag{9}$$

The mass matrix M and the inertia matrix K of the system can be obtained from the above equation, and the eigenvalue equation could be written as,

$$\Delta = \mathrm{K} - \omega^2 \mathrm{M} \tag{10}$$

The determinant of the above equation is of the 6th power of the frequency and remains 4th power the frequency after simplification, hence it contains a set of (two) natural frequencies. The natural frequency of the above system can be obtained by solving the determinant.

The displacement frequency response of the system could also be obtained,

$$\mathrm{H}_{\delta}(\omega) = \Delta^{-1} = (\mathrm{K} - \omega^2 \mathrm{M})^{-1} \tag{11}$$

The displacement transfer rate of the system could be written as,

$$\mathrm{T} = \left|\frac{\mathrm{u_f}}{\mathrm{u_p}}\right| = \left|\frac{\mathrm{u_t} + \mathrm{R_1 u_p}}{1+\mathrm{R_1}} \times \frac{1}{\mathrm{u_p}}\right| = \left|\frac{\mathrm{u_t}/\mathrm{u_p} + \mathrm{R_1}}{1+\mathrm{R_1}}\right| = \left|\frac{\mathrm{H_{21}}(\omega)/\mathrm{H_{11}}(\omega) + \mathrm{R_1}}{1+\mathrm{R_1}}\right| \tag{12}$$

According to the above theoretical formula, the overall low-order natural frequency $Mod_1$ and the high-low-order natural frequency $Mod_2$ of the designed dual-frequency vibration isolation system can be obtained for the coaxial helicopter. Assuming the motion energy of the system is absorbed by the vibration isolation system completely, the displacement of the fuselage mf approximately equals 0, and the displacement ratio at the upper and lower ends is a: b. Then the first-order anti-resonance frequency $fr_1$ and the second-order anti-resonance frequency $fr_2$ of the dual-frequency vibration isolation system could be obtained by the above eigenmatrix. (table 1)

**Table 1.** Performance calculation results.

| $k_1$ | $k_2$ | $m_t$ | $m_f$ | $m_p$ | $m_2$ | $Mod_1$ | $Mod_2$ | $R_1$ | $R_2$ | $fr_1$ | $fr_2$ |
|---|---|---|---|---|---|---|---|---|---|---|---|
| 88339 | 15174 | 1.23 | 9.28 | 4.51 | 1.26 | 9.017 | 19.400 | 4 | 0.375 | 8.523 | 19.544 |

## 3. Parametric Influence Analysis

### *3.1. Influence Law of Parameters*

5 design parameters of the vibration isolator, each parameter of 5 different sets of parameter values are chosen to explore the influence on the performance of the vibration isolator and the magnitude of the impact between the parameters on the performance. The effects of parameters on the natural frequency, optimal vibration isolation frequency, and vibration isolation efficiency of the vibration isolator are discussed.

It is seen from figure 3 that the change of the stiffness of the secondary spring $k_2$ has a great impact on the optimal secondary vibration isolation frequency $fr_2$, and $fr_2$ increases with the increase of $k_2$. Figure 4 and figure 5 reveal that the change of ratio $R_1$ and $R_2$ will change the vibration isolation frequencies $fr_1$ and $fr_2$ simultaneously. As $R_1$

increases, $fr_1$ and $fr_2$ decrease at the same time. As $R_2$ increases, $fr_1$ decreases while $fr_2$ increases. As shown in figure 6 and figure 7, the change of the first-level mass $m_t$ and the second-level mass $m_2$ will change the optimal isolation frequency, and it will decrease with the increase of $m_t$ and $m_2$.

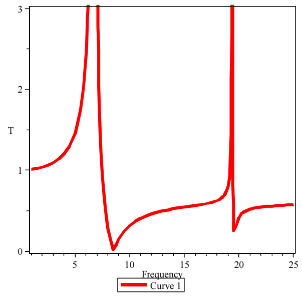


**Figure 2.** Calculation result of transfer function.

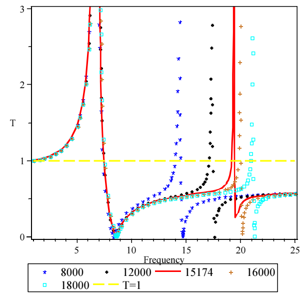


**Figure 3.** Influence of secondary spring stiffness.

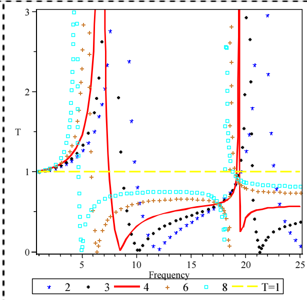


**Figure 4.** Influence of first-level amplification ratio.

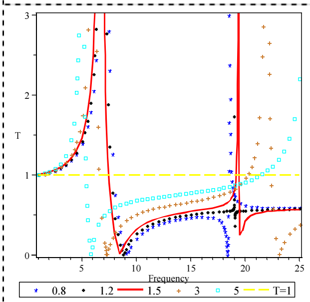


**Figure 5.** Influence of second-level amplification ratio.

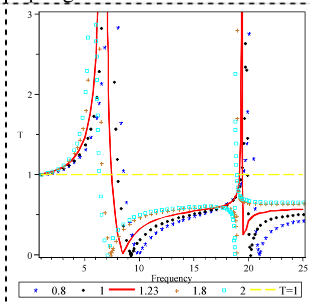


**Figure 6.** Influence of First-level mass block.

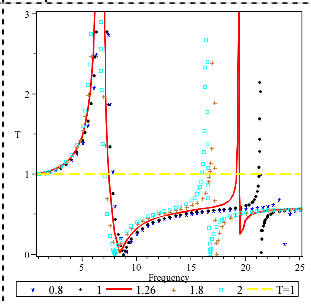


**Figure 7.** Influence of secondary mass block.

It is concluded from some figures (figure 4, figure 5, figure 6) that there would be the situation where the optimal second-level vibration isolation frequency $fr_2$ is less than the first-level natural frequency $Mod_2$. This phenomenon occurs when the magnification ratio is less than 1 or the mass is greater than the mass of the excitation。

### 3.2. Parameter Sensitivity Analysis

The influence of the five design parameters on the optimal vibration isolation frequency of the dual-frequency vibration isolation system has been obtained in the above section. Then the orthogonal test method is employed to analyze the effects of $k_2$, $R_1$, $R_2$, $m_t$, $m_2$ on the natural frequency of the system. The parameters of the orthogonal test table are as follows in table 2:

**Table 2.** Orthogonal test table.

| level | $k_2$ | $R_1$ | $R_2$ | $m_t$ | $m_2$ | level | $k_2$ | $R_1$ | $R_2$ | $m_t$ | $m_2$ |
|---|---|---|---|---|---|---|---|---|---|---|---|
| A | 8000 | 2 | 0.8 | 0.8 | 0.8 | B | 12000 | 3 | 1.2 | 1 | 1 |
| C | 15174 | 4 | 1.5 | 1.23 | 1.26 | D | 16000 | 6 | 3 | 1.8 | 1.8 |
| E | 18000 | 8 | 5 | 2 | 2 | | | | | | |

**Table 3.** Orthogonal test results.

| No. | $k_2$ | $R_1$ | $R_2$ | $m_t$ | $m_2$ | $Mod_1$ | Mod2 | $fr_1$ | $fr_2$ |
|---|---|---|---|---|---|---|---|---|---|
| 1 | A | A | A | A | A | 7.9 | 10.8 | 9.4 | 31 |
| 2 | A | B | B | B | B | 4.7 | 8.4 | 4.8 | 11 |
| 3 | A | C | C | C | C | 3.2 | 6.9 | 3.1 | 7.7 |
| | | | | | … | | | | |
| 25 | E | E | D | B | C | 3.5 | 9.4 | 3.3 | 9.7 |

Assuming that the above parameters are independent of each other and there is no coupling effect, then the natural frequency and the optimal vibration isolation frequency of the system under different parameter combinations could be obtained as in the orthogonal test table 3.

Applying the above orthogonal test result table, the average values of the test index under each level of each parameter are specified, and then the range of the test index average value under the same parameter at different levels could be calculated. Then the influence of each parameter on the natural frequency and the optimal vibration isolation frequency is obtained by comparing the magnitude of the range. The greater the range, the greater the sensitivity of the parameter to the result, and vice versa.

Taking orthogonal calculation result of the low-order natural frequency $Mod_1$ as an example, the range analysis results of $Mod_1$ are as follows.

**Table 4.** Results of range analysis for low-order natural frequencies.

| | $k_2$ | $R_1$ | $R_2$ | $m_t$ | $m_2$ | | $k_2$ | $R_1$ | $R_2$ | $m_t$ | $m_2$ |
|---|---|---|---|---|---|---|---|---|---|---|---|
| Group A | 4.02 | 4.54 | 4.88 | 3.24 | 3.01 | Group B | 3.75 | 3.96 | 3.75 | 3.14 | 3.34 |
| Group C | 3.58 | 3.41 | 3.87 | 3.91 | 3.59 | Group D | 3.56 | 3.59 | 3.11 | 4.06 | 4.09 |
| Group E | 3.98 | 3.39 | 3.29 | 4.55 | 4.87 | Average | 3.78 | 3.78 | 3.78 | 3.78 | 3.78 |
| Range | 0.89 | 1.88 | 2.38 | 2.36 | 2.80 | | | | | | |

As seen from table 4, the parameters of the index system that influences the low-order natural frequency $Mod_1$, the sensitivity in descending order would be the second-level mass $m_2$, the second-level amplification ratio $R_2$, the first-level mass $m_t$, and the first-level amplification ratio $R_1$, secondary spring stiffness $k_2$. Similarly for $Mod_2$, the sensitivity in descending order would be $k_2$, $R_2$, $m_2$, $m_t$, and $R_1$.

Also for $fr_1$, the sensitivity in descending order would be the second-level mass $m_2$, the second-level amplification ratio $R_2$, the first-level mass $m_t$, and the first-level amplification ratio $R_1$, secondary spring stiffness $k_2$. And last for $fr_2$, the sensitivity in descending order would be $m_t$, $R_1$, $R_2$, $m_2$, and $k_2$.

## 4. 3 Experiments on the Isolator

### *4.1. Design and Manufacture of the Isolator*

To verify the correctness of the established vibration isolation design and analysis method, and evaluate the vibration reduction efficiency of the dual-frequency vibration isolator at the vibration isolation frequency point accurately, experiments on the vibration reduction efficiency of the dual-frequency vibration isolation system are carried out.

Only the vertical motion is included in the theoretical model derivation process, the translation of the system and the rotation of the lever are ignored, considering the feasibility of the experiments, the dual-frequency vibration isolators are symmetrically arranged to reduce the impact of the movement caused by the incoordination of the plane (as shown in figure 8).

The upper and lower mass blocks in figure 1 are simulated by steel blocks. The lever is made of steel and the middle is slotted. The first-level isolation mass mt is replaced by a round mass plate and is connected to the slot with a bolt, and the second-level vibration isolation mass $m_2$ is connected to the spring $k_2$ made of aluminum alloy. The first-level spring $k_1$ is replaced by an aluminum alloy thin plate. The position of the bolt is changed to modify the installation points of the first-level and second-level substructure, resulting in different amplification ratios of the lever(as shown in figure 9).

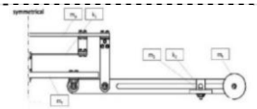

**Figure 8.** Design diagram.

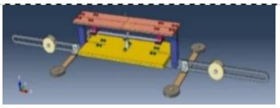

**Figure 9.** Model diagram.

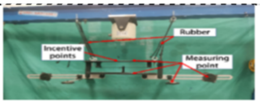


**Figure 10.** Performance test.

*4.2. Performance Test*

Experiments are conducted to verify the performances of the specimen. Two rubber ropes are connected to the upper mass block of the test piece and are symmetrically hoisted on the fixed truss. The upper mass block of the test piece is excited by a force hammer. Acceleration sensors (shown in figure 10) are mounted on the upper mass block, the first-level mass, the second-level mass, and the lower mass block. And the frequencies and modal shape data of the dual-frequency vibration isolation system are then acquired.
The natural frequencies and corresponding modal shapes are shown in figure 11-figure 14 below:

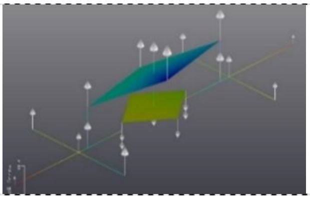

**Figure 11.** First-order natural frequency.

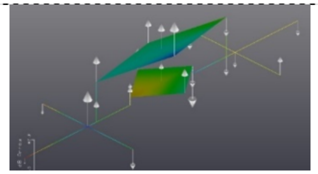

**Figure 12.** Second-order X-direction antisymmetric natural frequency.

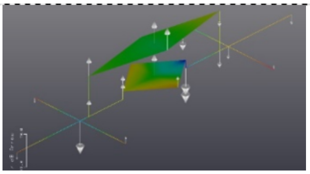

**Figure 13.** Third-order Y-direction antisymmetric natural frequency.

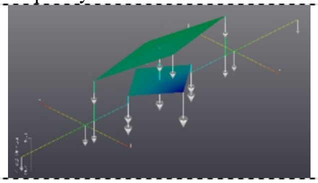

**Figure 14.** Fourth-order natural frequency.

According to the above figures, due to the symmetrical configuration, there are two antisymmetric modes (torsional modes) between the first and fourth modes of the vibration isolator sample. The following research work will focus on the overall modes of the vibration isolation system corresponding to the first and fourth orders modes, and the influences of the parameters are studied. With the aid of the frequency and mode shape analysis, the first-order natural frequency and mode shape corresponds to the low-order natural frequency $Mod_1$, and the fourth-order mode corresponds to the high-order natural frequency $Mod_2$.

The modal shapes at the two vibration isolation frequency points are shown in figure 11 and figure 14. Results demonstrate that the test could meet the requirement of the two vibration isolation frequencies of the dual-frequency vibration isolation system. The first-order and second-order natural frequencies are 8.2852 and 16.4599 respectively, with a relative error of 8% and 15%compared to the theoretical results in section 1.2. The main cause for the minor error lies in the employment of the small angle and no friction assumptions in the simplified model, and the masses of the lever and the spring itself are also ignored. Therefore, the correctness of the previous theoretical modeling could be verified from the perspective of the two natural frequencies.

### *4.3. Vibration Isolation Test*

Displacement transfer characteristics test and vibration isolation efficiency test are carried out in this section, the vibration isolation performance of the designed dual-frequency vibration isolator is evaluated. The accelerations of the upper and lower mass plates of the dual-frequency vibration isolation test were tested under different excitation loads.

By extracting the motion results of the upper and lower mass plates, the frequency response curves of the upper and lower mass plates are acquired, as shown in figure 15, where the solid red line represents the upper mass plate and the blue dashed line is the lower mass plate.

Dividing the response of the lower plate by the response result of the upper plate, the transmission rate curve under two excitation load tests are obtained and shown in figure 16. It can be seen that the first-order vibration isolation frequency is about 10.89, and the vibration transmission rate is about 0.84. The second-order vibration isolation frequency is about 16.05, and the vibration transmission rate is about 0.38 (vibration isolation effect is about 62%). It is also concluded from the figure that the best vibration isolation frequency point keeps unchanged under different excitation conditions. However, the vibration isolation efficiency (transmission rate T) is different. The reason is thought to be that the vibration isolation device may not vibrate normally under a small load state due to the existence of rotational friction and system damping.

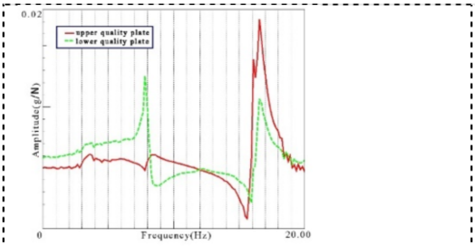


**Figure 15.** Frequency response function curve of upper and lower quality plate.

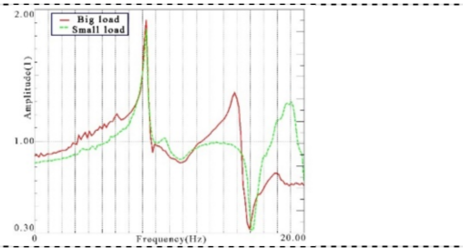


**Figure 16.** Curve of excited vibration transfer rate under different loads.

Keeping the excitation load unchanged, the influence of the mass position of the counterweight on the frequency response function is tested by changing the position of the first-level mass block $m_t$. The response curves are shown in figure 17.

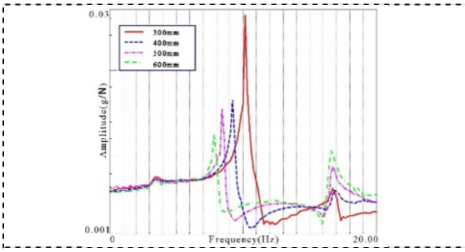


**Figure 17.** Influence of first-order damping mass position on the frequency response function.

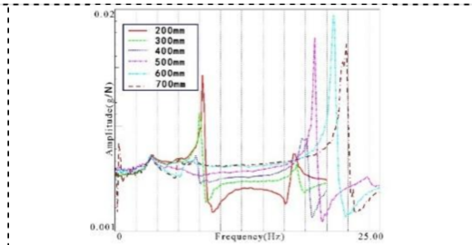


**Figure 18.** The influence of the position of the spring on the frequency response function.

It can be seen from the above curves that changing the position of the first-level vibration mass $m_t$ not only changes the optimal low-order vibration isolation frequency point but also affects the vibration isolation efficiency of the first-level vibration isolation frequency point, which is consistent with the aforementioned parametric analysis. Compared with the first-level vibration isolation frequency, the position of the first-level vibration mass $m_t$ has less influence on the second-level vibration isolation frequency point, however, it affects the vibration isolation efficiency. The reason for this phenomenon is that the high-order vibration isolation frequency is mainly determined by $m_2$ and $k_2$ and is relatively more independent. But the vibration isolation efficiency is still affected by the dynamic characteristics of the entire system, therefore it is also affected by the position of $m_t$.

Changing the position of the spring $k_2$ (which affects the magnitude of $R_2$) and the other conditions keeps unchanged, the results are illustrated in figure 18. The position of the spring $K_2$ has a little influence on the low-order vibration isolation frequency points but has a great influence on the response of the high-order vibration isolation frequency points and the first and second level vibration isolation frequency points, which is in line with the aforementioned calculation results. The main cause for this phenomenon is that the secondary vibration system participates in the lower-order (first level) vibration reduction procedure as a subsystem, and also performs as the primary system for second-level vibration reduction at the same time.

It could also be seen from figure 17 and figure 18 that there will be the case where the optimal secondary vibration isolation frequency $fr_2$ is smaller than the higher-order natural frequency $Mod_2$, which is identical to the aforementioned analysis.

## 5. Conclusions

A dual-frequency passive vibration isolator with two-level vibration isolation frequencies is designed, based on the theory of dynamic anti-resonance to meet the future demand of vibration isolation for dual main vibration frequencies. Theoretical analysis and experiments are performed to explore the inherent characteristics of the vibration isolator and verify the vibration isolation effectiveness. Results demonstrate a 62% second-level vibration isolation rate of the vibration isolator.

The natural frequency and effects of parameters on the optimal vibration isolation frequency of dual-frequency vibration isolator are obtained through parameter influence analysis and changing parameters test. Different parameters imply different impacts on the two-level optimal vibration isolation frequencies and the natural frequencies. The magnitude of the vibration isolation efficiency is affected by the design parameters.

## References

[1] LU Yi. Vibration and Vibration Reduction Technology of Helicopter, China Science and Technology Review, 2009, 000(001):89-89.

[2] Peter F L, Gary K L, John J O. Overview of S-97 RaiderTM Scale Model Tests. AHS 72th Annual Forum, West Palm Beach, FL, May 2016, 3109-3125.

[3] YU Zhi-hao, ZHOU Yun, SONG Bin. Aeroelastic modeling and load analysis of a variable speed rotor in high advance ratio. Journal of Vibration and Shock, 2021, 40(4):17-22.

[4] George J, Farhan G. Investigation of Performance Loads and Vibrations of a Coaxial Helicopter in High Speed-Flight. AHS 72nd Annual Forum, West Palm Beach, Florida, May 17–19, 2016, 1402-1417.

[5] Walsh D, Weiner S, Arifian K,et al. High airspeed testing of the sikorsky X2 technology demonstrator, AHS 67nd Annual Forum, Virginia Beach, VA, May 4, 2011, 2999-3010.

[6] Zhang Wen, Zhang Fang, Jiang Jin-hui. Control algorithm design and simulation for active DAVI system[J]. Foreign Electronic Measurement Technology, 2015(10):17-21.

[7] Smith M R, Lee T, Merkley D J. Active Vibration Treatment for Rotorcraft with Piezo-Live Technolog[C], 61st Annual forum of the American Helicopter Society, 2005, 107-116.

[8] Chen Yong, David G Z. Research of an active tunable vibration absorber for helicopter vibration control. Chinese Journal Of Aeronautics, 2003, 16(4):203-211.

[9] ZHANG Chi, YU Guang-dong, YUE Chao-song, Vibration Isolating Study on a Centrifugal Fan Noise Controlling System used in a Mine Wind Well, Noise And Vibration Control, 2005, 25(5):68-69.

[10] LIN Chang-liang, XIA Shuang-man, ZHANG Ti-lei,et al. Adjustable stiffness structure application in helicopter vibration reduction. Journal of Vibration Engineering, 2019, 32(6):950-955.

[11] MA Xun-jun, LU Yang, CHEN Ren-liang,et al. Multi-frequency helicopter vibration control method using parallel-form adaptive filters. Journal of Vibration Engineering, 2016, 29(5):755-764.

[12] LIU Niu-niu, ZHANG Zhen-guo, XU Shi-yin,et al. Local resonance bandgap of a periodic slender beam based on dynamic anti-resonance structure. Journal of Vibration and Shock, 2017, 36(24):142-147